Monthly Notices
of the
ROYAL ASTRONOMICAL SOCIETY

MNRAS **469,** S492–S505 (2017)
Advance Access publication 2017 August 2

doi:10.1093/mnras/stx1908

Similarities in element content between comet 67P/Churyumov–Gerasimenko coma dust and selected meteorite samples

Oliver J. Stenzel,[1]★ Martin Hilchenbach,[1] Sihane Merouane,[1] John Paquette,[1] Kurt Varmuza,[2] Cécile Engrand,[3] Franz Brandstätter,[4] Christian Koeberl,[4,5] Ludovic Ferrière,[4] Peter Filzmoser,[2] Sandra Siljeström[6] and the COSIMA team

[1]*Max Planck Institute for Solar System Research, Justus-von-Liebig-Weg 3, D-37077 Göttingen, Germany*
[2]*Vienna University of Technology, Institute of Statistics and Mathematical Methods in Economics, A-1040 Vienna, Austria*
[3]*Centre de Sciences Nucléaires et de Sciences de la Matière – CSNSM, Bat. 104, 91 405 Orsay, France*
[4]*Natural History Museum, Burgring 7, A-1010 Vienna, Austria*
[5]*Department of Lithospheric Research, University of Vienna, A-1090 Vienna, Austria*
[6]*RISE Research Institutes of Sweden, Bioscience and Materials / Chemistry and Materials, Box 5607, 114 86 Stockholm, Sweden*

Accepted 2017 July 25. Received 2017 June 26; in original form 2017 February 21

ABSTRACT

We have analysed the element composition and the context of particles collected within the coma of 67P/Churyumov–Gerasimenko with Rosetta's COmetary Secondary Ion Mass Analyzer (COSIMA). A comparison has been made between on board cometary samples and four meteorite samples measured in the laboratory with the COSIMA reference model. Focusing on the rock-forming elements, we have found similarities with chondrite meteorites for some ion count ratios. The composition of 67P/Churyumov–Gerasimenko particles measured by COSIMA shows an enrichment in volatile elements compared to that of the investigated Renazzo (CR2) carbonaceous meteorite sample.

Key words: comets: individual: 67P/Churyumov–Gerasimenko – meteorites, meteors, meteoroids.

1 INTRODUCTION

In this work, we discuss the results of analyses of the relative element composition of cometary particles captured in the inner coma of comet 67P/Churyumov–Gerasimenko (hereafter 67P) and compare the results with analyses of meteorite samples in the laboratory. The COmetary Secondary Ion Mass Analyser (COSIMA) is a time-of-flight secondary ion mass spectrometer on board the Rosetta spacecraft and was analysing cometary particles ejected from the nucleus of comet 67P since 2014 August (Kissel et al. 2007; Hilchenbach et al. 2016). The study of returned Stardust samples have highlighted the presence of many components similar to those found in carbonaceous chondrites (CC), albeit at smaller scales, mixed with material that originated in the outer Solar system and pre-solar grains (Brownlee 2014). In contrast to CC compositions, Wild 2 particles showed no sign of aqueous alteration (Zolensky et al. 2006). To understand the composition and the history of the collected cometary 67P particles, the results obtained from these grains have been compared with the characteristics of different meteorite samples, which have been analysed with the COSIMA reference instrument at the Max Planck Institute for Solar system Research in Göttingen (Germany), a Time of Flight Secondary Ion Mass Spectrometer (ToF-SIMS) IV at Research Institute of Sweden (RISE) in Bårs, Sweden, and with SEM-EDX at Natural History Museum Vienna, Austria. The goal has been to better understand how the cometary particles compare to well-known bodies from the Solar system, and to get to know how primitive they are and whether alteration is visible from the relative element content.

COSIMA uses a Time of Flight Secondary Ion Mass Spectrometer (ToF-SIMS) for characterizing the surface of samples. The primary ion source has a beam footprint of 35 by 50 μm (full width at half-maximum) and though the particle is visible in front of its target background and some variation within the particle show on ion images (see e.g. Fig. 3 of Hilchenbach et al. 2016), the spatial resolution is too low to isolate individual crystals or structures like inclusions in the grains. Thus, we focus in this work on bulk constituents of the cometary particles that we have sampled from the coma of 67P. The COSIMA SIMS has a mass resolution, $m/\Delta m$, of 1400 at 100 u which allows for a distinction between peaks of hydrogen-rich organic compounds and peaks of mineral compounds and elements at the same nominal mass. The SIMS process does not directly yield absolute abundances, because the ion yields are dependent on type of species, matrix and primary ion beam used (Benninghoven, Rudenauer & Werner 1987). Therefore, we have focused on the analysis of the ratios between the secondary ion

★ E-mail: stenzel@mps.mpg.de

Table 1. Comet and meteorite samples used in this work.

Sample	67P	Renazzo	Murchison	Allende	Lancé	Tieschitz	Ochansk	Tissint
Type of meteorite	/	CR2	CM2	CV3	CO3.5	H/L3.6	H4	Shergottite
Mass of original sample / g	/	0.089	1.544	0.524	0.083	0.330	0.725	0.143
NHMV sample ref. #	/	ID_6468_[1]	ID_5840_[2]	ID_426_[1]	ID_3594_[1]	ID_7906_[1]	ID_7907_[1]	ID_7994_[11]
Total number spectra	1388	50	132	447	121	50	100	150
# of spectra in ion ratios	693	32	28	46	62	40	25	31
# of background spectra	279	10	25	87	35	10	20	30

counts for the respective elements and compounds for the different samples.

For the interpretation of the results it is therefore necessary to choose comparable reference samples. As we are interested in the cosmochemical context of the comet particles, meteorite samples are an appropriate choice.

Comparing the SIMS results for the cometary particles with results for meteorite samples measured with the same instrument in the laboratory has the great advantage of circumventing the inherent problem of absolute calibration of the instrument. Calibration of the element sensitivities, relative sensitivity factors (RSF), for a SIMS instrument is very dependent on the matrix of the sample at hand (Krüger et al. 2015). The element abundances ratio with regard to Fe of 67P particles relative to CI carbonaceous chondrites have been analysed showing variations between particles as well as highlighting variations within cometary particles and finding two possible calcium-aluminum-rich inclusions (CAI; Hilchenbach et al. 2016; Paquette et al. 2016). In this work we focus on the bulk abundances, i.e. the ion ratios, from which the composition of individual particles can deviate. Both previous papers compare their results to CI element abundances (Lodders 2010).

2 MATERIALS AND METHODS

An overview of the cometary and meteoritic samples is given in Table 1.

2.1 Cometary particles

The cometary particles investigated in this study were collected between 2014 December and 2015 February at solar distances of 2.74–2.39 au and at 20–108 km distance from the centre of the nucleus. The particles were collected on a metal target plate (named '2CF', Fig. 1a). The target plate is covered with gold black, a deep black surface. COSIMA had 24 target holders each carrying three such targets for dust collection with different kinds of coatings (Hornung et al. 2014). The target 2CF was exposed 19 times. The typical exposure times were 1–7 d. Most of the particles on this target plate are classified as shattered or glued clusters and rubble piles, indicating that the particles broke up on impact (Langevin et al. 2016), and very few compact particles have been collected on this target. Particles equal to or larger than 14 μm could be identified. The size range of collected particles is 14–800 μm. The particles typically arrive in bursts and at least for the clustered class, stick to the target (Hornung et al. 2016; Merouane et al. 2016). COSIMA was able to collect coma particles travelling at higher nucleocentric velocities than 0.5 ms^{-1}. Slower particles could not enter through the funnel because of the relative spacecraft velocity as described in Merouane et al. (2016). The GIADA instrument measured the cometary particles velocities of 0.3 ms^{-1}–12.2 ms^{-1} (Della Corte et al. 2015). COSIMA was able to collect incoming cometary particles over most of their velocity range.

2.2 Meteorite samples

Seven samples of different types of meteorites from the collection of the Natural History Museum Vienna (NHMV) have been used for this study. The samples have been taken from seven stony meteorites: Renazzo, Murchison, Allende, Lancé, Tieschitz, Ochansk and Tissint (Wiik 1956; Mason & Wiik 1962; King et al. 1969; Michel-Lévy 1969; Kurat 1970; Jarosewich 1971; Chennaoui Aoudjehane et al. 2012). These meteorites were chosen to represent a wide range of meteorite types, mineral composition, origin and history. Four belong to the group of carbonaceous chondrites: Renazzo is a CR2, Murchison is a CM2, the most primitive meteorite in our set, Allende is a CV3 and Lancé is a CO3.5. Tieschitz is a H/L3.6 unequilibrated ordinary chondrite that has seen less thermal metamorphism than Ochansk, another ordinary chondrite of H4 type. All these meteorites have the same age as the Solar system. Tissint originates from the youngest body, among all samples, as it is a Martian meteorite (shergottite) (Brennecka, Borg & Wadhwa 2012). We have included Tissint, the only achondrite in our set, as a control sample, with the full knowledge that such rock types are not represented among comets. The compositional difference with regard to the chondrites serves as a yardstick when comparing the cometary particles.

The bulk element composition of Renazzo can be found in Kallemeyn & Wasson (1982), Kallemeyn, Rubin & Wasson (1994), for Murchison, Allende and Lancé in Kallemeyn & Wasson (1981), for Tieschitz in Kallemeyn et al. (1989); Schmitt et al. (1972), for Ochansk in Wiik (1956); Easton & Elliott (1977), and for Tissint in Chennaoui Aoudjehane et al. (2012) and Liu et al. (2016).

All meteorite samples were gently crushed in a petri dish and small fragments were pressed on a 1 cm^2 COSIMA blank gold target (Fig. 1b).

The samples that we have prepared are a few hundreds of micrometre in size and therefore do not necessarily have the same composition as the bulk meteorite. In order to characterize the meteorite samples that were analysed by the COSIMA instrument, the same samples were also investigated with a number of other techniques. After measurements with the COSIMA reference model (see Section 2.3), the same meteorite samples have been analysed with a commercial ToF-SIMS IV (ION-TOF GmbH), a Raman microscope and with a scanning electron microscope (SEM).

The SEM Jeol JSM-6610LV, located at the NHMV, is equipped with an energy-dispersive X-ray (EDX) system with a Bruker XFlash detector operated through Esprit microanalysis software. All SEM investigations were carried out on uncoated (i.e. without carbon coating) samples. To minimize charging effects, backscattered electron (BSE) images were taken in the so-called low vacuum

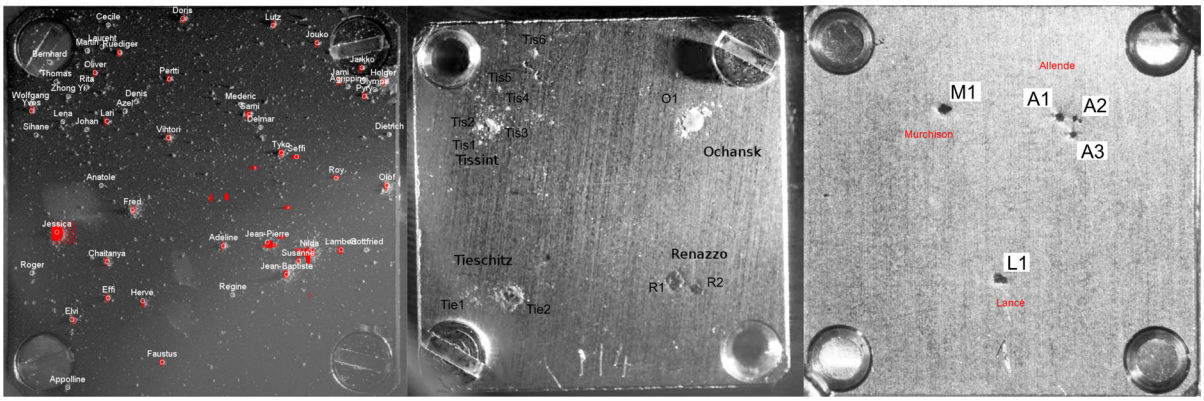

Figure 1. (a) Target 2CF from the COSIMA XM with cometary material collected between 2014 Dec and 2015 Feb inside the inner coma of 67/P. Particles with an area of more than 36 square pixels are marked with their name. The approximate positions of the SIMS locations are marked with red circles. (b) Target 4E1 from the COSIMA RM with four meteorite samples (1 CC, 2 OC and 1 Shergottite). (c) Target 4B7 (COSIMA RM) with three CC samples. The size of the plates is 1×1 cm^2.

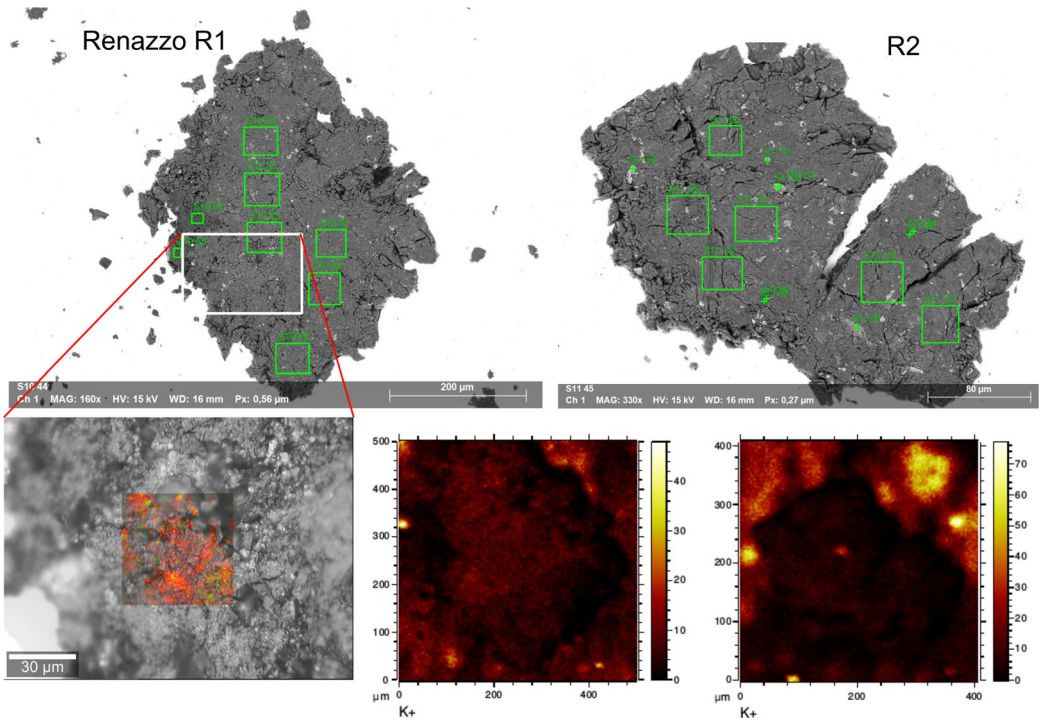

Figure 2. Overview of different measurements done on the Renazzo sample. Top row: Backscatter electron images of two Renazzo grains (lower right corner of target 4E1 in Fig. 1b). Note that the grains are presented in a different scale; grain R1 is larger than grain R2. The green markings show the places at which EDX measurements were obtained. Bottom row: Raman results for olivine (green), and oxides (red) for the Renazzo grain R1. The potassium ion counts images, measured by the ION-TOF ToF-SIMS IV instrument, for both grains are presented on the right side of the Raman results.

mode. EDX-analyses of the meteorite grains were performed under high-vacuum conditions at 15 kV accelerating voltage and 150 pA probe current. In total 167 positions on 16 meteorite grains have been analysed. For comparison with the bulk element content of Renazzo the larger measurement areas of 160 µm^2 and 250 µm^2 on grains R1 and R2 have been used to obtain atomic abundances of a number of elements. We have converted those to relative mass abundance. The top row of Fig. 2 shows the positions of X-ray analysis in green squares.

The Raman microscope is a Witec Alpha 3000 equipped with a 532 nm laser, located at MPS in Göttingen. Mappings were acquired with a 50x objective, leading to a lateral resolution of about 1.5 μm. The integration time is 0.2 second per spectrum. The mapping acquired on Renazzo has a lateral dimension of 50 × 50 µm and a resolution of 0.4 × 0.4 µm. The mapping of Tieschitz has a lateral dimension of 160 × 160 µm and a resolution of 1 × 1 µm.

High-performance ToF-SIMS analyses of meteorites were performed with a ToF-SIMS IV instrument (ION-TOF GmbH, Germany), located at Research Institute of Sweden in Borås, Sweden. Samples were analysed by rastering a 25 keV Bi_3^+ beam over a 500 × 500 µm^2 area for 200 s. The analyses were performed in both positive and negative ion mode at high mass resolution (bunched mode: $m/\Delta m \geq 7000$ at m/z 30, $\Delta l \approx 5$ µm) with a pulsed current of 0.1 pA. To simulate COSIMA conditions, the

sample surface was not flooded with electrons for charge compensation, even though samples were charging.

2.3 The COSIMA ToF-SIMS spectra

COSIMA is a time-of-flight secondary ion mass spectrometer that uses positive indium ions at 8 keV energy for its primary ion beam. One model of COSIMA, the XM (for eXchange Model) is on board the Rosetta spacecraft, while another, the RM (Reference Model) is located at the Max Planck Institute for Solar system Research in Göttingen (Germany). COSIMA XM can expose metal target plates for dust collection at the end of a funnel which is open to the cometary coma. The target plates are moved between different stations inside the instrument by the robotic Target Manipulation Unit (TMU). After selected collection periods, the target plates are moved from the funnel to the microscope camera COSISCOPE to image the target. The illumination of the target is from either the left side or the right side. The images are analysed on the ground. Newly collected particles are registered in a catalogue and names are assigned (at least for the largest particles) in order to facilitate the discussion about them (Fig. 1a). Their position as acquired from the optical images have been used to plan the *in situ* mass spectrometry measurements. For analysis with the ToF-SIMS, the target is moved by the TMU in front of the secondary ion lens (SIL) of the spectrometer unit of COSIMA. An 8 keV pulsed ion beam hits the particles and target at an ellipse of about 35 × 50 μm full width at half-maximum. The secondary ions sputtered from the surface are accelerated by applying a positive or negative electric field and fly through a time-of-flight tube before hitting the detector. The spectrum is typically collected for 2.5 min integration time and is thereafter mass calibrated and down linked to ground. A detailed description of the instrument can be found in Kissel et al. (2007). The SIMS can be operated in either positive or negative secondary ion mode. In this work, only positive spectra were considered, which are the most representative for the analysis of most rock-forming elements. The COSIMA spectra are already well calibrated when they are downloaded from the instrument, but slight differences in the mass scales between spectra can broaden the peaks when adding a large number of spectra. To retain as much resolution as possible during the summation of the spectra, we have re-calibrated all the spectra on ground. All spectra are dead-time corrected and fitted to a reference spectrum, specially chosen for its good absolute mass calibration. The XM spectra taken at the positions of the particles generally show a much lower total ion yield than spectra taken on the target background. We interpret this as a consequence of the porous inner structure of the comet particles (Hilchenbach et al. 2016). The approximate SIMS positions are marked by red circles. This work is based on 1434 spectra accumulated on these positions in Fig. 1a. The spectra amount to roughly 58 h of SIMS. To get good counting statistics and to obtain bulk values for the comet and the meteorites, several spectra have been added for each of the samples (Table 1).

The mass spectra from the XM and RM show different secondary ion yields and different contamination peaks. Therefore, the spectra need to be normalized for comparison. For normalization, we have used the gold peak (target substrate in both cases) at $m/z = 196.97$ u. Fig. 3(a–h) shows a comparison of the different samples for the m/z interval of 0.5 u–150 u on a linear ion count scale. Characteristic for this instrument is the high baseline produced by ions from different elements and molecules, especially at the higher masses. This background scales with the secondary ion counts. Fig. 4(a) shows a smaller part of the same spectra at a logarithmic ion count scale (51.5 u $\leq m/z \leq$ 58.5 u). Peaks to the right of the integer mass are generally from organic ions, in this case mostly originating from contamination from the target, while the peaks left of the integer mass are mostly element ions originating from the samples. In particular, the $^{56}Fe^+$ peak for all our samples, the $^{58}Ni^+$ peak for Renazzo and the $^{52}Cr^+$ peaks for Tissint and Ochansk are obvious. The mass resolution of the instrument is nominally high enough to distinguish between the 'organic' (H-rich) ions on the one hand, and the elements and hydrogen-poor molecules on the other hand. The mass resolution is also high enough to recognize different contributions from $^{56}Fe^+$ and $^{28}Si_2^+$, even though the peaks are not separated. Assuming the left shoulder peak at mass 54 u is $^{54}Fe^+$, the inorganic peak at 56 u can be explained almost entirely as $^{56}Fe^+$ by the isotopic ratio of iron. The $^{28}Si_2^+$ contribution is seen as small right shoulder on the Fe peak. The Poisson-statistics mean that the generally high contamination peaks will get wider, and signals from less abundant or less easily ionized elements or molecules might only appear as shoulders or artificially broadened peaks. We see this behaviour for, e.g. potassium and calcium in the mass spectra of our comet particle (Fig. 4b). The contamination is generally higher in the XM spectra than in the RM spectra.

2.4 Ion ratios

In total, 1434 XM spectra were measured between 2015 December and the end of 2016 April for cometary particles on target 2CF. From those, we first excluded the measurements on top of the screw in the top right corner of the target, as the composition of the screw is visible in the spectra (Fig. 1a). Then, we selected those spectra that were measured mostly on a particle, in total 693 spectra. This is a non-trivial task, as many spectra contain information from both the particle and the surrounding target, because of the width of the primary ion beam foot print. Magnesium is nearly absent on the target but is found in the cometary particles (Hilchenbach et al. 2016). Therefore, the ratio between Mg and the target substrate, which in this case is gold, is a good indication of how much of the signal originates from the grain or the target. In ion images generated from the spectra, we see that Mg is present in all the particle positions analysed on target 2CF. Therefore, it is unlikely that a bias has been introduced into the results by selecting only Mg-bearing particles. However, since the primary ion beam has a larger lateral extension than the size of most particles, the signal from small particles is always mixed with the background and there is no cut-off value at which to make a clear on/off distinction. For the spectra on target 2CF on the XM, we have tested several Mg/Au cut-off values and found that choosing the median of the Mg/Au ratio distribution yields a value at which the information in the spectra is mainly originating from the particles. Using stricter criteria, e.g. the 80 per cent percentile of the Mg/Au distribution, yields negligible differences in the results. Using the 50 per cent criterion still excludes some spectra that contain cometary contributions and still includes some contamination, albeit at a reduced level.

In contrast to the mostly organic contamination (PDMS) present on the XM target, the target plates used in the RM are also contaminated with material containing Na, K and Ca. This can be seen e.g. in the potassium ion images for the Renazzo grains measured on the ION-TOF instrument (Fig. 2). The criteria for the selection of RM meteorite spectra are different from that of the selection of cometary 2CF spectra. The following criteria were used for the meteorite samples: Renazzo and Tieschitz: Mg/Au larger or equal to the 20 per cent quantile, Ochansk: a matrix of scans chosen by hand since Mg/Au criteria have not been successful, Tissint: Mg/Au larger or equal to the 80 per cent percentile. Murchison: Mg/Au

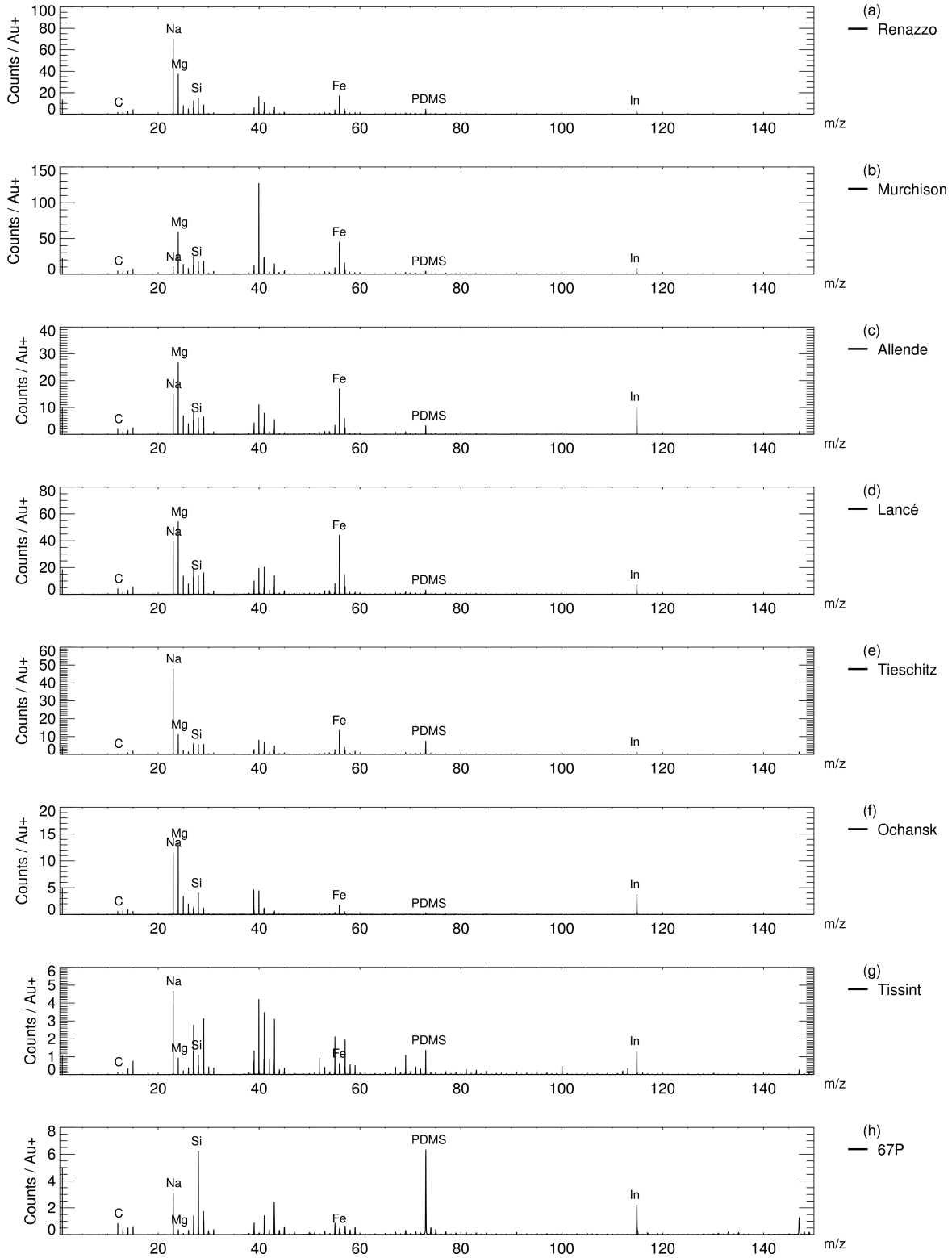

Figure 3. Summed spectra for the seven meteorite samples and the comet particles. All spectra were normalized to the sum of five channels centred at $m/z = 196.97$ u (Au^+). (a)–(h) show the m/z range between 0 and 150 u.

larger or equal to the 80 per cent percentile, Allende: Mg/Au larger or equal to the 90 per cent percentile and Lancé: Mg/Au larger or equal to the 50 per cent percentile.

To remove the background, the normalized background was subtracted from the selected meteorite and cometary spectra. For the XM, we have used the spectra that have an Mg/Au value that is less than, or equal to, the 20 per cent percentile of the Mg/Au distribution as background spectra. For the RM, the background spectra that are in close proximity to the meteorite sample and lower or equal to the 20 per cent percentile have been used. The close distance on

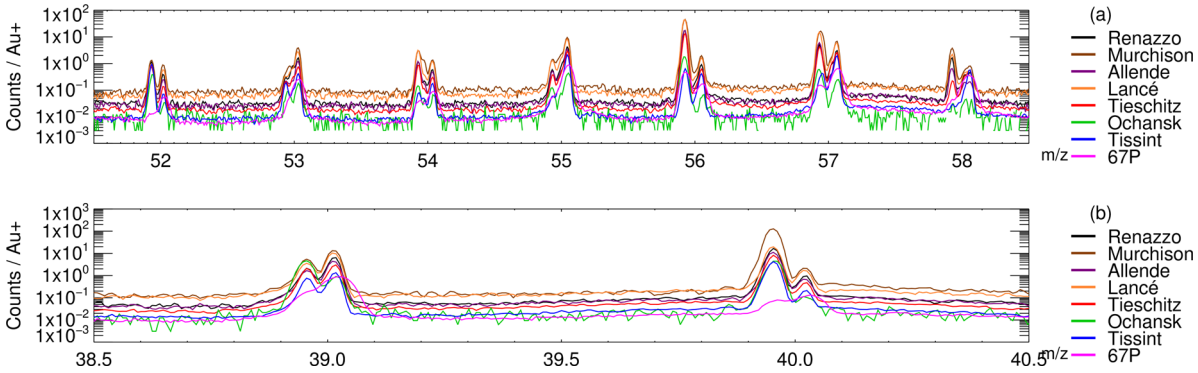

Figure 4. Summed spectra for the seven meteorite samples and the comet particles. All spectra were normalized to the sum of five channels centred at $m/z = 196.97$ u (Au^+). (a) shows the m/z range between 51.5 and 58.5 u, and the ordinate in logarithmic scale. The peaks to the right of the integer mass are generally organic contamination from the target, while the peaks left of the integer mass are mostly elements from the samples. In particular, the ^{56}Fe peak for all our samples, the ^{58}Ni peak for Renazzo and the ^{52}Cr peaks for Tissint and Ochansk are visible. (b) shows the m/z range between 38.5 and 40.5 u in logarithmic scale. Peaks to the right of the integer mass are organic contamination from the target, while the peaks to the left of the integer mass are potassium and calcium from the samples.

the target of background spectra to the meteorite grains in the RM is essential as some elements are present both, in the sample, and in strongly varying amounts on the target. On the XM target, this does not effect the results as much as the variation in the RM target. There are only a few elements in the XM spectra that show significant contribution from both the target and the particles: C, Si and S. The contamination on the XM targets is not uniform, but this variation is cancelled by averaging.

The first step in calculating the ion ratios from the selected spectra is adding the on-sample and background spectra, respectively. The peaks at a given mass are usually the sum of contributions from different elements, compounds and instrument artefacts. These artefacts are different for the XM and RM. To be able to compare the element contributions, it is necessary to de-convolute these peaks. We fit a series of Gaussians with the Levenberg–Marquardt algorithm to each of those peaks to isolate the contribution of each element of interest. Up to four peaks can be fitted this way at each integer mass. The integral over the fitted Gaussian peak is used for calculating the ion ratios and abundances after subtracting the local background:

$$N_{\rm net} = N_{\rm measured} - B\frac{P}{P_{\rm B}},$$

where $N_{\rm net}$ is resulting ion count, $N_{\rm measured}$ is the measured ion count on the sample, B is the ion count of the local background on the target plate, P is the ion count of gold and $P_{\rm B}$ on the target.

The relative elemental abundances are presented normalized to Fe. For normalization, any element can be chosen from the mathematical point of view. All relative abundances are just shifted by a constant factor if another element such as Mg or Si are chosen. In our case, we preferred Fe as it is not affected by any contamination and present in the overall majority of the mass spectra of the samples. This normalization method was sometimes also used in studies of Stardust samples that were collected in silica aerogel, or in the case of IDPs collected in silicon oil.

To get an estimate of the variations within the samples, the average abundance and standard deviation have been estimated via bootstrapping (Efron 1979). This means that the abundances are calculated repeatedly from many randomly chosen subsets of the data and then the result is averaged. The standard deviation represents the variability of the abundances throughout the sample. The sub-sample size is $n_{\rm S} = 10$ and the number of sets drawn is $n_{\rm D} = 99$.

Ternary diagrams have been prepared for further comparison of the ion ratios (Figs 5a–d). Since COSIMA only measures the elemental composition, ternary diagrams give hints on the possible mineralogical composition in the sample. These diagrams are internally normalized (i.e. the sum of the 3 end-members add to 100 per cent), so a combination of several ternary diagrams should be used to minimize the risk of wrong interpretation. Each point for a given sample source represents one of the abundances calculated in the bootstrapping process. These diagrams are used for the comparison between different samples, as absolute abundances are not used. Thus, the relative abundances between the elements might be biased, but they are biased in the same way for all samples, provided that the matrix effects in cometary and meteorite samples are similar.

3 RESULTS

3.1 Meteorite sample characterization

The meteorite samples have been analysed with a ToF-SIMS IV (Renazzo and Tieschitz, only), a Raman-spectrometer, and with a scanning electron microscope using backscattered electron (BSE) images and X-ray spectrometry (EDX). Figs 6, 2 and 7 show the Raman and EDX spectra locations on the samples. Table 2 gives an overview of the results.

3.1.1 Tieschitz

Fig. 6 shows an example for the multi-instrument analysis for one of the Tieschitz grain Tie2. The Raman-spectrometer detects olivine (green markings in Fig. 6) and additionally pyroxene (blue) and oxides (red). The ToF-SIMS IV and BSE images of Tie2 show basically two different domains in the grain, one Mg rich and one Fe rich. Tie2 is an extremely heterogeneous fragment consisting mainly of Fe-Mg-silicates (olivine and low-Ca pyroxene), feldspathic matrix material and iron sulfide (troilite). The troilite-dominated area apparently is one single sulfide aggregate that was partly crushed during preparation.

The Tieschitz grain Tie1 is dominated by Fe-Mg-silicates (olivine and low-Ca pyroxene) with much less abundant feldspathic matrix material and scattered grains of iron sulfide (troilite).

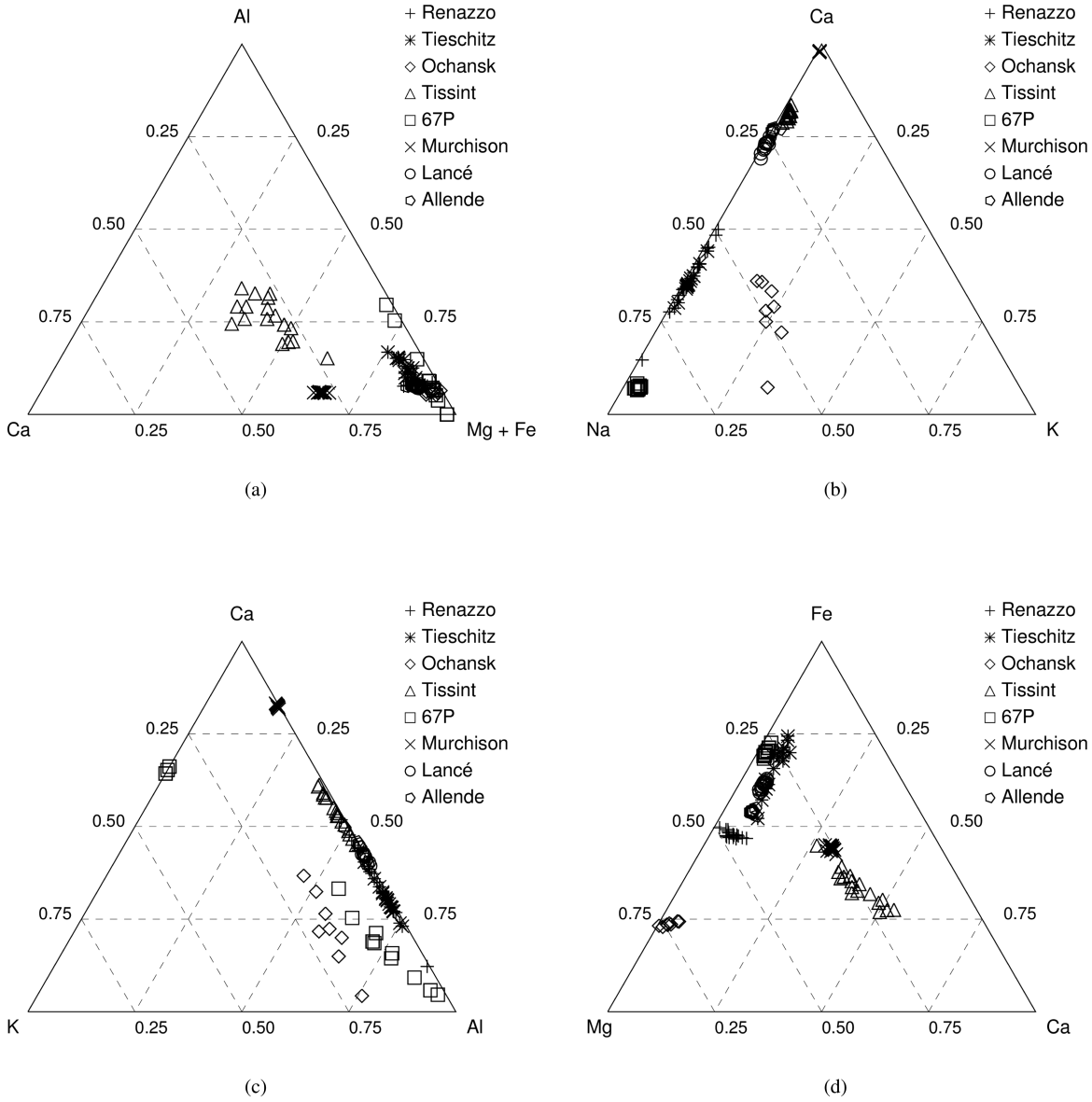

Figure 5. Ternary diagrams of element abundances. Each data point marks the average abundance over a randomly chosen set of spectra from a specific sample (see the text). (a) compares calcium, magnesium + iron and aluminum abundances, (b–c) feldspar-forming element abundances and (d) major rock-forming element abundances.

Compared to the bulk abundances of Tieschitz, the sample is slightly enriched in Na, Al, K, Ca and Mn and depleted in Ni with regard to Fe (Fig. 8, light blue. The FeS phase was not included in the EDX bulk measurements).

3.1.2 Renazzo

ToF-SIMS IV, Raman and BSE analyses all show fine-grained material (Fig. 2). The Raman spectra show mainly olivines and oxides. EDX 'Bulk analyses' performed on $\sim 50 \times 50$ μm-large areas on R1 have rather uniform compositions and exhibit elevated element contents in S and Ni. One ~100 μm-large olivine grain has a forsteritic (= high Mg) composition. R2 consists mainly of fine-grained matrix material. In comparison with fragment R1 it appears slightly enriched in opaques (iron sulfide and/or nickel-iron metal). 'Bulk analyses' performed on $\sim 40 \times 40$ μm-large areas approximately have uniform compositions.

When comparing the EDX results with the bulk element abundances by Kallemeyn et al. (1994), we find a good agreement between the 'bulk measurements' on the Renazzo grains and the Renazzo bulk content, with the exceptions of Na and K. These two elements are overabundant in the samples analysed in the RM (Fig. 8, dark green).

3.1.3 Murchison

The Raman spectra show pyroxenes mixed with magnetite.

The grain M1 consists approximately half of a coarse-grained aggregate (individual domains > 100 μm) and half of a fine-grained matrix material (grain size < 10 μm). Compositionally, the coarse-grained aggregate consists mainly of probably hydrated Ca-sulfate (gypsum). The fine-grained matrix consists of an intimate intergrowth of different silicate and/or oxide phases. In places, isolated grains of forsteritic (Mg-rich) olivine occur. The Murchison sample

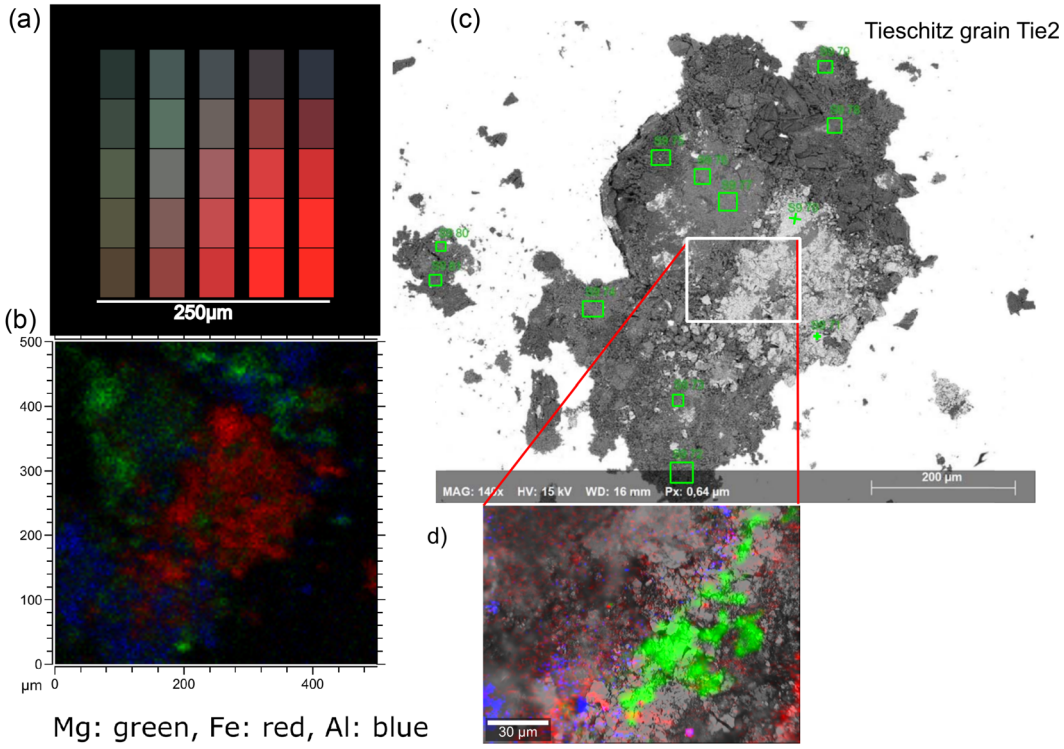

Figure 6. Comparison of results for the Tieschitz sample with different instruments. The left column shows the SIMS analysis with the COSIMA reference model (a) and the ION-TOF instrument (b) for Mg, Fe and Al, marked in green, red and blue, respectively. The right column shows the backscatter electron image (BSE) (c) and for the inlaid region the Raman spectroscopic results (d) for olivine (green), pyroxene (blue) and oxides (red), the green rectangles mark the positions of the X-ray spectra.

is richer in Fe than the bulk meteorite, all compared elements (Na, Mg, Al, K, Cr, Mn and Ni) apart from Ca are depleted relative to Fe. Looking only at the fine-grained phase of grain M1, a depletion of Ca/Fe can be seen, too (Fig. 8, dark blue and brown symbols).

3.1.4 Allende

The Allende sample consists of four grains that show in the EDX spectra mainly olivines of uniform composition, some (Fe,Ni)-sulfides and a few Mg-rich pyroxenes and olivine fragments. The Raman spectrum analysis on a 40 µm square of grain A1 yields a mixture of olivine and magnetite with little pyroxene and sulfates. The sample is depleted in Na/Fe, Mg/Fe, Al/Fe, Ca/Fe, Mn/Fe and Ni/Fe, while Cr/Fe is on the same level as the bulk meteorite (Fig. 8, red symbols).

3.1.5 Lancé

The Raman spectrum shows coarse to fine-grained olivine with minor amounts of pyroxene, and even lower amounts of magnetite.

L1: Fragment, consisting mainly (about 4/5 of the total area) of a rather uniform, fine-grained silicate matrix that is intergrown with a coarser-grained heterogeneous lithology. In the fine-grained matrix a few scattered grains of (Fe,Ni)-metal and Fe-sulfide occur. "Bulk" analyses show that olivine of intermediate composition is the dominant mineral of the fine-grained matrix whereas in the coarser-grained lithology forsteritic olivine is more abundant. The Lancé sample is depleted in Na/Fe, Al/Fe, K/Fe, Ca/Fe and Ni/Fe. Mg/Fe, Cr/Fe and Mn/Fe are within one standard deviation from the bulk values (Fig. 8, dark yellow symbols).

3.1.6 Ochansk

From the Raman measurements the presence of olivine, pyroxene, Fe-oxides and feldspars can be seen. The EDX finds that the Ochansk fragment (just one grain, O1) is dominated by Fe-Mg-silicates (olivine and low-Ca pyroxene) and fine-grained feldspathic matrix material – indicated by significant contents of Na and Al. In places, iron sulfide (troilite) forms larger grains. Some areas are dominated by olivine. All elements in the comparison but Ni show higher abundance with regard to Fe than the bulk abundances (Fig. 8, black).

3.1.7 Tissint

The Raman measurements show mainly pyroxene with some spots of olivine on grain Tis3. Tis2 also shows pyroxene and a second, hard to identify, possibly amorphized phase. Six Tissint grains have been analysed with EDX: Tis1: Coarse-grained silicate fragment consisting mainly of olivine. Less abundant are augitic pyroxene and 'plagioclase'. Tis2: Coarse-grained silicate fragment consisting mainly of 'plagioclase' and minor augitic pyroxene. Tis3: Coarse-grained silicate fragment consisting mainly of 'plagioclase'-rich components, augitic pyroxene and olivine. Tis4: Coarse-grained silicate fragment consisting mainly of 'plagioclase' and augitic pyroxene plus one isolated grain of olivine. Tis5: Coarse-grained silicate fragment consisting mainly of augitic pyroxene and less abundant 'plagioclase'. Tis6: Coarse-grained silicate fragment consisting mainly of augitic pyroxene.

The Tissint sample shows within one standard variation agreement between the EDX measurements and literature values for the bulk composition (Fig. 8, light green).

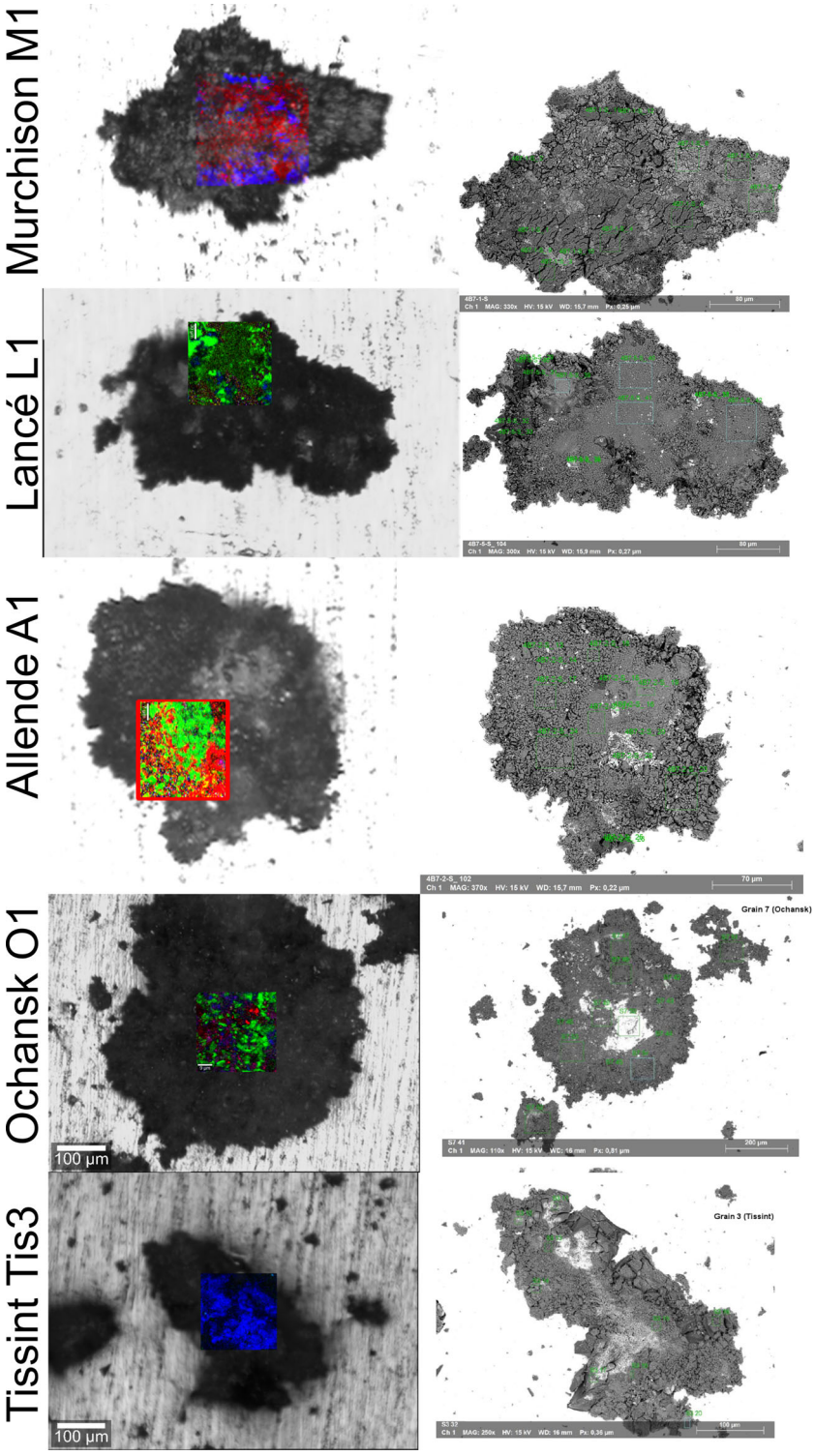

Figure 7. Positions of Raman (left column) and EDX measurements (right column). Raman mappings are given for olivine, pyroxene, iron oxides and feldspars, and sulfates in green, blue, red, purple and yellow, respectively.

3.2 COSIMA ion ratios

The normalized sum spectra for the comet particles and the meteorite samples are presented in Fig. 3. Fig. 3a–h shows the part of the spectra between 0 and 150 u in linear scale. All spectra have been normalized to the intensity of the Au peak. Some peaks of interest are labelled. The cometary spectra show higher contamination with PDMS fragments than the meteorite sample spectra. Figs 4(a) and (b) show narrower mass ranges of the same spectra in logarithmic scale to illustrate the peaks of the elements Cr, Mn, Fe and Ni (Fig. 4a), and K and Ca (Fig. 4n). For some of these elements, there are interferences from other elements or molecules, for example the peak at $m/z = 40$ u is not only Ca^+ but can also have contributions

Table 2. Overview of laboratory instrument results on mineral composition of the meteorite samples.

Sample	Renazzo	Murchison	Allende	Lancé	Tieschitz	Ochansk	Tissint
Structure	fine-grained	50/50 per cent fine – and coarse grained	fine-grained fragments	mostly uniform fine-grained matrix	heterogeneous, fine and coarse grained mixture	mostly fine-grained	coarse-grained
EDX	mostly uniform	gypsum, silicates and oxides	olivine	olivine, intermediate mixture, coarser phase is forsteric	olivine, pyroxenes, troilite	olivine, pyroxene, feldspar	olivine, pyroxenes, 'plagioclase'
Raman	FeO and olivine	pyroxene and magnetite	olivine and magnetite	mostly olivine, some pyroxene	olivine, pyroxenes, oxides	olivine, pyroxene, feldspar, oxides	pyroxenes

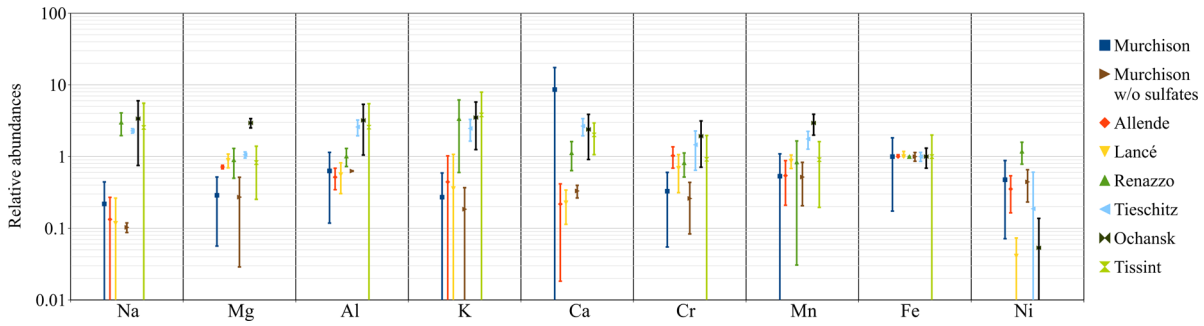

Figure 8. EDX results for all meteorite samples compared with bulk element content by Kallemeyn et al. (1994), Kallemeyn & Wasson (1981) and Liu et al. (2016). The error bars represent the standard deviation of the EDX measurements squares shown e.g. for Renazzo in Fig. 2. The Murchison sample consists of mainly two phases, one of which is calcium sulfate, the other is mainly matrix material. The measurements with and without the calcium-rich phase are shown.

from MgO^+, with the peak maxima that should be separated by two time bins. The maximum of the peak matches the theoretical Ca^+ peak almost perfectly for all samples, while MgO^+ coincides with a local minimum. The oxides have generally a much lower yield in the positive ion mode of the instrument so we made the assumption that the peak at mass 40 is mainly Ca^+. At $m/z = 56$ u, where the major iron peak is expected, Si_2^+ and CaO^+ ions are present but they do not contribute to the measured peaks intensity for more than ≈1 per cent, estimated from the intensity of the ^{54}Fe isotope.

The ion yield of elements is generally much higher for elements than molecular ions for the COSIMA instrument. Section 2 describes, in detail, how the ion ratios for the cometary and meteorite samples are computed. The results can be seen in Fig. 9. The elements are sorted from most volatile to least volatile (Davis 2006; Lodders 2003). The siderophile elements are marked in red, lithophile elements are marked in blue and chalcophile elements are marked in green. The error bars give the range of ± two standard deviations from the bootstrapping process described in Section 2.4. The large error bars that extend downwards to the edge of the figure are due to individual bootstrapping sets that did not yield a result for the respective element. Not every element is detected in every sample. The reason for this is not necessarily their absence but rather the low intensities and high background level. Fig. 9a shows the ion ratios of the cometary particles relative to the Renazzo sample $(X_{67P}/Fe_{67P})/(X_{Ren}/Fe_{Ren})$. There is a negative trend in the ion ratio values with decreasing volatility evident with one exception: a high Si/Fe ratio, which is about 10 times higher for the cometary samples than for the Renazzo sample. Also the carbon and sulfur ratios show enrichments by a factor of 10 compared to Renazzo. The aluminum is the least volatile element under investigation. The Al/Fe ratios are rather similar in the cometary particles and in the Renazzo meteorite. Fig. 9b–g shows the ion ratios observed between 67P particles and the other meteorite samples. Compared with the other carbonaceous chondrites, 67P shows the same general trend as with the Renazzo sample. The ratios relative to the Tieschitz sample behave mostly like the CCs, while the ratios relative to the Ochansk sample show much larger deviations in the K/Fe and Mg/Fe ratios.

3.3 Ternary diagrams

Four ternary diagrams have been prepared to compare the compositional similarities and differences between the samples in terms of mineralogically related elements (Figs 5a–d). Fig. 5(a) shows the sets of each sample in the compositional triangle of Ca, Mg+Fe and Al. All chondrites samples, except for Murchison and the comet samples are crowded into the Mg+Fe corner. 67P shows some spread due to varying Al or Ca + Al content. Murchison and Tissint form distinct groups of higher Ca content.

Fig. 5(b) shows the ternary diagram for different feldspar-forming elements: Na, K and Ca. Most samples can be found along the Na – Ca line. Ochansk ratios centre around $(Na_{0.5}, K_{0.25}, Ca_{0.25})$, probably related to the feldspar content visible in Raman and EDX analysis. The Tissint, Allende and Lancé samples all plot at high Ca values. Murchison shows isolated at the Ca corner. Fig. 5(c) compares the feldspar elements K, Al and Ca. The Allende, Renazzo, Lancé, Ochansk and Tissint samples situated at the Al – Ca line, with Murchison far removed towards the Ca corner. Ochansk and 67P samples show higher values of K and form a separate group.

In the comparison of the composition in terms of the major rock building elements Mg, Ca and Fe (Fig. 5d), there is a trend from Fe-rich with 67P and Tieschitz on one end to Mg-rich with Ochansk at the other end. Murchison and Tissint are again separated from the others due to high Ca content. The high Fe content of Tieschitz sample was expected because of its FeS phase. The Ochansk sample

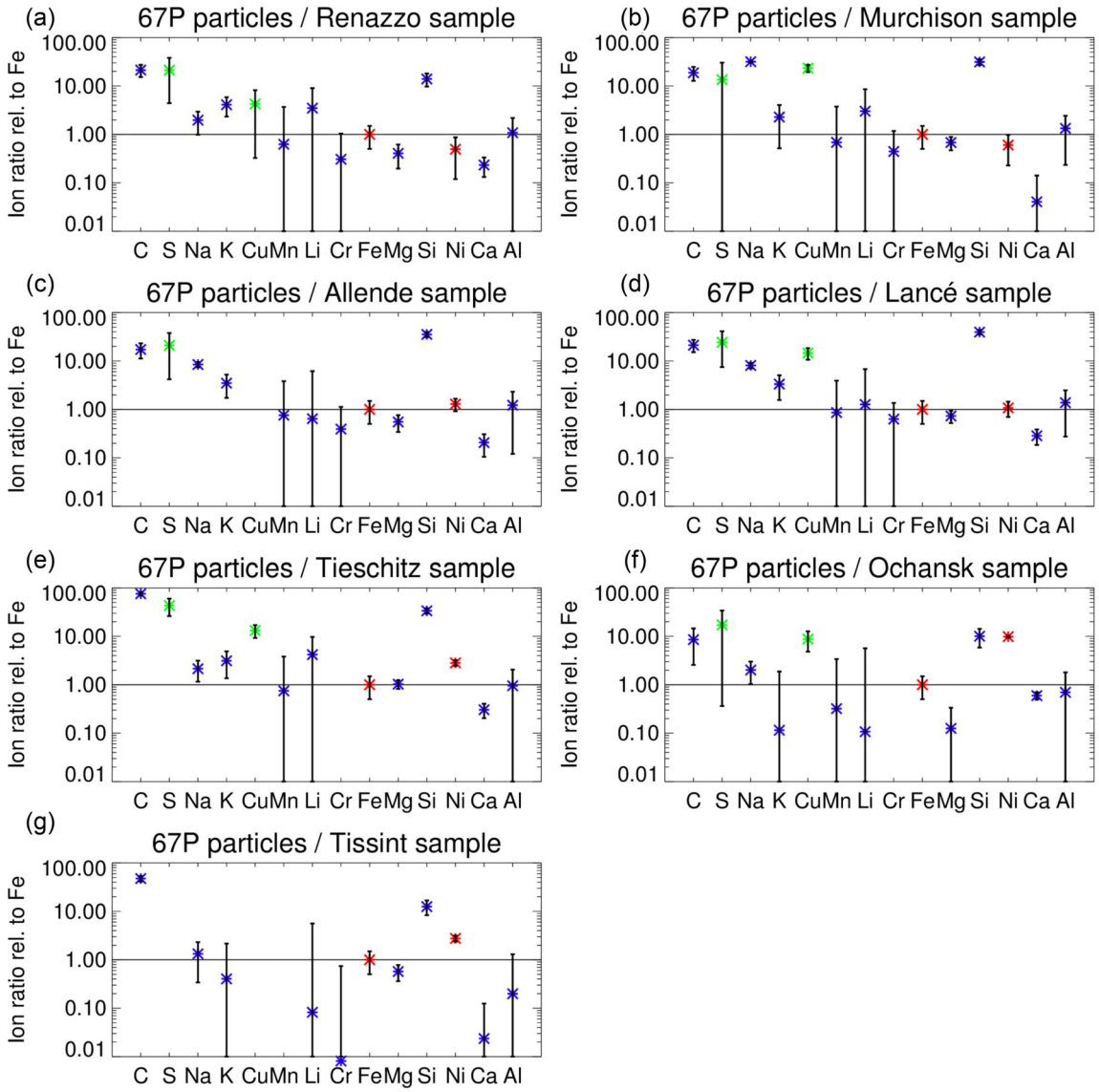

Figure 9. Ion ratios of elements found in the cometary particles, relative to the meteorite samples. The target background was subtracted for all elements. Siderophile, chalcophile and lithophile elements are marked in red, green and blue, respectively.

has a very high Mg abundance relative to the bulk meteorite (see Section 3.1).

4 DISCUSSION

4.1 Element ratios

The bulk ion ratios for the cometary particles are generally close to the results from the carbonaceous chondrites and Tieschitz and to a lesser degree with Ochansk. They are far from the shergottite Tissint sample. There is an enrichment of the volatile elements C, S, Na, K, Cu and Li in the cometary particles compared to Renazzo and Tieschitz samples (Fig. 9a and 9e). A relatively clear trend of decreasing relative abundance with decreasing volatility is observed. Variation from this trend and large uncertainties appear for the elements Cu, Mn, Li and Cr. The low abundances, especially of Li and Cu, however, limit further conclusions.

Schulz et al. (2015) and Hilchenbach et al. (2016) both report high abundances of Na for the cometary particles in calibrated ratios or compared to CI level. They were calibrated with relative sensitivity factors (RSF) from Krüger et al. (2015), so they are not directly comparable to the values from Fig. 9. With applied RSF values, an Na/Mg ratio of about 0.4 is obtained for the data set in this work and 0.8 and 0.2–1.7 in Schulz et al. (2015) and Hilchenbach et al. (2016), respectively. Wurz et al. (2015) used the Rosetta Orbiter Spectrometer for Ion and Neutral Analysis (ROSINA) Double Focusing Mass Spectrometer (DFMS) instrument on board Rosetta to measure element ions sputtered from the surface of 67P. They measured a Na/Si ratio of 0.021, half of the CI value. Jessberger, Christoforidis & Kissel (1988) measured an Na abundance for Comet Halley's dust that is twice the CI level. We see an enrichment of Na compared to the meteorite samples in this study. Since the Na abundance in the meteorite samples might be slightly overestimated because of contamination as discussed in Section 2.4, the Na ratios for the comet compared to the meteorites, e.g. $(Na/Fe)_{67P}/(Na/Fe)_{Ren}$ might in fact be lower limits.

The aluminum-to-iron ratio is approximately the same in the cometary as in the Renazzo, Tieschitz and Ochansk samples. We

interpret this as an upper limit because of possible contributions from $C_2H_3^+$ ions. The peak fitting described in Section 2.4 works well, but cannot completely eliminate the interference of the much larger C_2H_3 peak. In the meteorite samples this is not a problem, as there is better separation of the two peaks.

K is even more abundant in the comet particles than Na relative to the Renazzo and Tieschitz, but not to the Ochansk and Tissint samples. The tail of the organic peak at mass 39 u ($C_2H_3^+$) contributes to the K counts. As discussed for the Al, the peaks are fitted and the tail of the neighbouring organic mass should not play a large role anymore.

The cometary particles show magnesium to iron ratios at the same level as for the Tieschitz sample and lower ones than for the Renazzo sample. In the ternary diagram of Mg, Ca and Fe, 67P and Tieschitz form a group with Lancé (Fig. 5d). Allende and Renazzo are closer to Mg. The Tieschitz sample covers a wider range between Fe and Mg than other samples, because of its FeS phase. The Ochansk sample is detached towards the Mg corner. It has a much higher Mg/Fe ratio than the bulk meteorite (Fig. 8). The high iron content with regard to Mg and Ca in the comet particles can be interpreted as an enrichment of Fe bearing silicates like fayalite (Fe_2SiO_4) or ferrosilite ($Fe_2Si_2O_6$) and troilite (FeS) compared to the CC samples or as a matrix effect.

The Ca/Fe ratio of the comet is close to Ochansk, and the lowest within our samples. Ca/Fe is found to be at about 0.2 times the Renazzo, Allende and Lancé values in this work, while other works with COSIMA show slightly higher values than CI Ca/Fe content (Hilchenbach et al. 2016; Paquette et al. 2016). This is likely due to selecting especially Ca-rich spectra in Paquette et al. (2016), as these were the regions of interest and Hilchenbach et al. (2016) found just two particles within their selection with Ca, but these at a high level.

The C and Si overabundance in cometary material could be interpreted as partly due to contamination of the target plate with PDMS. Note that we subtract the background and even if not all background contribution for these elements is eliminated, most of the signal probably is from the cometary particles.

The BSE image of the Tieschitz sample shows two compositionally different phases (Fig. 6). EDX analysis showed that one is a silicate and the other likely is troilite. The sulfur abundance seen in the EDX spectra on Tieschitz however, is very low in the RM ToF-SIMS data, probably due to low sensitivity in the positive mode for S, especially when it is present as FeS. After subtracting the background from the target, no residual S can be seen from that phase. Fig. 9e shows that the S/Fe ion ratio is much larger in the comet particles than in the Tieschitz sample. Therefore, it is likely that another source for the S exists in the comet.

Recently, Fray et al. (2016) concluded the presence of high molecular weight refractory organic matter in 67P dust particles, reminiscent of insoluble organic matter (IOM) found in carbonaceous chondrites like Orgueil and Murchison. The analyses of 67P dust particles however show a higher hydrogen content in the organic phase than for the meteoritic IOM, suggesting a more pristine nature of the cometary organic matter. This observation is compatible with our results regarding the rock composition of the cometary particles from 67P.

4.2 Clues on minerals

The mineral composition of the cometary particles is difficult to infer from only relative abundance information. The ternary plots in Figs 5(a)–(d) give hints that the mineral compositions are close to those of the Renazzo and Tieschitz samples and, to a lesser degree, to the Ochansk one. The Tissint sample is very different from the other samples because it is a differentiated meteorite.

The relatively high amounts of Na and K suggests the presence of feldspar minerals in the cometary particles. Possible candidates for the source of Na in the comet are sodium silicates nepheline ($NaAlSiO_4$) and albite ($NaAlSi_3O_8$) and there is probably orthoclase feldspar ($KAlSi_3O_8$) present in the cometary sample, explaining the comparably high K/Fe ratios. In the ternary plot of K, Al and Ca we see that the 67P particle ion ratios group with the Ochansk sample (Fig. 5c), with the ternary plot of Na, K and Ca this is not the case. If the alkali metals in the 67P particles are mainly from feldspars, they have different endmember ratios than in Ochansk. Na might have additional sources apart from feldspars. Salts are possible candidates. Halogens are abundantly found in the negative spectra (not used in this work, and hard to disentangle from the background) and we see a high abundance of sulfur, which can originate from sodium sulfate. However, salts in meteorites mostly originate from crystallization from brines of precursors like feldspars and sodalite ($Na_4[AlSiO_4]3Cl$) instead of condensation in the protoplanetary cloud. Rubin, Zolensky & Bodnar (2002) analysed halite grains in two ordinary chondrites, Monahans (1998) and Zag, and concluded that the grains formed early (within a few million years of accretion) on their parent bodies possibly by leaching of alkalies of chondrule mesostases and Cl from chlorapatite grains. Na_2O might be found in amorphous silicates, which could be present. The Renazzo and Tieschitz grains contain both olivine and (low calcium) pyroxene (Section 3.1), it is likely that these are also present in the cometary particles.

The Mg/Fe depletion with regard to Renazzo hints at Fa- rather than Fo-rich olivines. A depletion of Mg-rich minerals could have different reasons. It is for e.g. possible that the mineral constituents of the cometary particles formed directly by recondensation in an environment that was already depleted in Mg and forsterite (Palme & Fegley 1990). Another possibility would be the aqueous alteration of silica and FeO in the already condensed grains (Wasson & Krot 1994).

4.3 Implications of the similarities and differences

Fig. 9 showed that many elements show similar ion ratios as the CC meteorites with a general trend with regard to the volatility of the elements. The global exception for this trend is Si, which is elevated in 67P compared to all other samples. Looking at the trend of decreasing abundance with decreasing volatility indicates less thermal processing in the case of the cometary sample data, as thermal heating would preferentially remove volatile elements from the cometary particles. In this regard, the cometary particles from 67P appear to be the most 'primitive' of the samples in this study, though it should be emphasized that the meteorite samples considered for this study do not cover the full range of meteorite classes, and that the composition of a single sub-mm sized sample might vary a lot from the bulk meteorite composition. The characterization of the meteorite samples with BSE imaging and EDX shows indeed a heterogenic mineralogy and element distribution for many of the samples and especially for the second Tieschitz grain, which consists of silicates and a large troilite inclusion. This larger scale heterogeneity is even visible in the RM TOF-SIMS results (Fig. 6). The two Renazzo grains are far more homogeneous (Fig. 2). The comparison with the meteorite's bulk content shows that most of the elements that were analysed in both this work and in Kallemeyn et al. (1994) show identical abundances within one sigma (Fig. 8).

There are only differences in Na and K, with Na more than one sigma higher in our sample. Na and K are both present as contaminations on the target and as presented in Section 2, we need to subtract this contamination background when analysing the SIMS results. This gives us some confidence that we indeed compare our cometary data with a decent representation of the Renazzo meteorite and its class. Of course other elements might differ. The other CC samples are generally elevated in Fe abundance compared to the bulk meteorite.

The largest differences between the CC samples and the 67P particles are higher C/Fe, S/Fe and Si/Fe ratios in the comet and the lower Mg/Fe and Ca/Fe ratios. A mixture of two phases originating from different parts of the protoplanetary disc/early Solar system that was accumulated during the early stages of cometesimal formation might also explain, why these elements are much more abundant in the comet than in carbonaceous chondrites.

Carbonaceous chondrites have suffered extensive aqueous alteration on the parent body, that could have remobilized soluble and carbonaceous phases, but there is no evidence for correlation between the concentration of potential soluble elements and the degree of aqueous alteration of carbonaceous chondrites. For CR meteorites there is even evidence that the organic matter is spatially associated with hydrated silicates, suggesting that organic matter was brought together with icy grains and stayed associated with the hydrated silicates (Le Guillou & Brearley 2014).

5 CONCLUSIONS

We have analysed the TOF-SIMS spectra of cometary material measured in space and compared the results with spectra of meteorite samples measured in the laboratory with the reference instrument. In the comet particles we find similarities with chondritic meteorites, which have comparable element ratios for many rock-forming elements. The enrichment in volatile elements (C, S, Na, K, Cu and Li) in the cometary particles compared to that of meteorites indicates less thermal processing in the cometary particles than for the other samples studied.

Apart from the silicate phase that shows reasonably good agreement with chondrites, the elements C, Si and S are much more abundant in the cometary particles than in the studied meteorites. This might partly be due to contamination, but the amount of the overabundance and the careful subtraction of the contamination background gives reason to assume that 67P is indeed much more abundant in C, S and Si than chondrites due to their origin in different parts of the protoplanetary disc.

For the other building blocks of chondritic material and under the condition that the CC sample abundances resemble the bulk abundances of their class well and to the extent that CC and CI abundances are comparable for many elements, we see a good agreement between the composition of the cometary particles reported here with previous work on COSIMA ToF-SIMS data from comet particles. Those studies, however, reported results for a fewer number of elements (Schulz et al. 2015; Hilchenbach et al. 2016; Paquette et al. 2016).

ACKNOWLEDGEMENTS

COSIMA was built by a consortium led by the Max-Planck-Institut für Extraterrestrische Physik, Garching, Germany in collaboration with Laboratoire de Physique et Chimie de l'Environnement et de l'Espace, Orléans, France, Institut d'Astrophysique Spatiale, Centre national de la recherche scientifique (CNRS)/Université Paris Sud, Orsay, France, Finnish Meteorological Institute, Helsinki, Finland, Universität Wuppertal, Wuppertal, Germany, von Hoerner und Sulger GmbH, Schwetzingen, Germany, Universität der Bundeswehr, Neubiberg, Germany, Institut für Physik, Forschungszentrum Seibersdorf, Seibersdorf, Austria, Space Research Institute, Austrian Academy of Sciences, Graz, Austria and is led by the Max-Planck-Institut für Sonnensystemforschung, Göttingen, Germany. We thank H. Fischer and H. Krüger for technical assistance in the COSIMA RM operations and sample handling. The support of the national funding agencies of Germany (Deutsches Zentrum für Luft- und Raumfahrt e.V. (DLR), Raumfahrtmanagement, grant 50 QP1302), France centre national d'études spatiales (CNES), Austria (Austrian Science Fund, FWF, project P 26871-N20), Finland and the European Space Agency (ESA) Technical Directorate is gratefully acknowledged. S. Siljeström acknowledges funding from the Swedish National Space Board (contracts 121/11 and 198/15). We thank the Rosetta Science Ground Segment at European Space Astronomy Centre (ESAC), the Rosetta Mission Operations Centre at European Space Operations Centre (ESOC) and the Rosetta Project at European Space Research and Technology Centre (ESTEC) for their outstanding work enabling the Science return of the Rosetta Mission. Rosetta is an ESA mission with contributions from its Member States and National Aeronautics and Space Administration (NASA).

REFERENCES

Benninghoven A., Rudenauer F. G., Werner H. W., 1987, Secondary ion mass spectrometry: basic concepts, instrumental aspects, applications and trends. John Wiley and Sons, New York
Brennecka G. A., Borg L. E., Wadhwa M., 2012, Meteorit. Planet. Sci. Suppl., id.5157
Brownlee D., 2014, Annu. Rev. Earth Planet. Sci., 42, 179
Chennaoui Aoudjehane H. et al., 2012, Science, 338, 785
Davis A. M., 2006, Meteorites and the Early Solar system II. Univ Arizona Press
Della Corte V. et al., 2015, A&A, 583, A13
Easton A. J., Elliott C. J., 1977, Meteoritics, 12, 409
Efron B., 1979, Ann. Statist., 7, 1
Fray N. et al., 2016, Nature, 538, 72
Hilchenbach M. et al., 2016, ApJ, 816, L32
Hornung K. et al., 2014, Planet. Space Sci., 103, 309
Hornung K. et al., 2016, Planet. Space Sci., 133, 63
Jarosewich E., 1971, Meteoritics, 6, 49
Jessberger E. K., Christoforidis A., Kissel J., 1988a, Nature, 332, 691
Kallemeyn G. W., Wasson J. T., 1981, Geochim. Cosmochim. Acta, 45, 1217
Kallemeyn G. W., Wasson J. T., 1982, Geochim. Cosmochim. Acta, 46, 2217
Kallemeyn G. W., Rubin A. E., Wang D., Wasson J. T., 1989, Geochim. Cosmochim. Acta, 53, 2747
Kallemeyn G. W., Rubin A. E., Wasson J. T., 1994, Geochim. Cosmochim. Acta, 58, 2873
King, Jr E. A., Schonfeld E., Richardson K. A., Eldridge J. S., 1969, Science, 163, 928
Kissel J. et al., 2007, Space Sci. Rev., 128, 823
Krüger H. et al., 2015, Planet. Space Sci., 117, 35
Kurat G., 1970, Earth Planet. Sci. Lett., 7, 317
Langevin Y. et al., 2016, Icarus, 271, 76
Le Guillou C., Brearley A., 2014, Geochim. Cosmochim. Acta, 131, 344
Liu Y., Baziotis I. P., Asimow P. D., Bodnar R. J., Taylor L. A., 2016, Meteorit. Planet. Sci., 51, 2293
Lodders K., 2003, ApJ, 591, 1220
Lodders K., 2010, in Goswami A., Reddy B. E., eds, Astrophys. Space Sci. Proc., Principles and Perspectives in Cosmochemistry. Springer-Verlag, p. 379

Mason B. H., Wiik H. B., 1962, American Museum Novitates, no. 2106
Merouane S. et al., 2016, A&A, 596, A87
Michel-Lévy M. C., 1969, in Millman P. M., ed., Astrophysics and Space Science Library Vol. 12, Meteorite Research. Springer, Netherlands, p. 492
Palme H., Fegley B., 1990, Earth Planet. Sci. Lett., 101, 180
the COSIMA TeamPaquette J. A., Engrand C., Stenzel O., Hilchenbach M., Kissel J., 2016, Meteorit. Planet. Sci., 51, 1340
Rubin A. E., Zolensky M. E., Bodnar R. J., 2002, Meteorit. Planet. Sci., 37, 125
Schmitt R. A., Goles G. G., Smith R. H., Osborn T. W., 1972, Meteoritics, 7, 131
Schulz R. et al., 2015, Nature, 518, 216
Wasson J. T., Krot A. N., 1994, Earth Planet. Sci. Lett., 122, 403
Wiik H., 1956, Geochim. Cosmochim. Acta, 9, 279
Wurz P. et al., 2015, A&A, 583, A22
Zolensky M. E. et al., 2006, Science, 314, 1735

This paper has been typeset from a TEX/LATEX file prepared by the author.